

Microstructure evolution of aluminum-lithium alloy 2195 undergoing commercial production

JIANG Na(蒋 呐)^{1,2}, GAO Xiang(高 翔)³, ZHENG Zi-qiao(郑子樵)¹

1. School of Materials Science and Engineering, Central South University, Changsha 410083, China;
2. Technical Center, Southwest Aluminum (Group) Corporation Limited, Chongqing 401326, China;
3. ARC Centre of Excellence for Design in Light Metals, Monash University, Clayton 3800, Australia

Received 22 February 2009; accepted 19 April 2009

Abstract: Microstructures of three kinds of typical product states for commercially fabricated alloy 2195 were observed. It is found that the hot-rolled plate is characterized by a fibrous structure containing fine, polygonized substructures; and the cold-rolled sheet was characterized by a “pan-caked” grain structure containing high density dislocation cells. The product under near peak-aging temper is proved to contain a large amount of dispersive, plate-shaped $T_1(\text{Al}_2\text{CuLi})$ precipitates, together with a small fraction of $\theta'(\text{Al}_2\text{Cu})$ plates, exhibiting a desirable combination of mechanical properties. Analyses using scanning electron microscopy reveal that many coarse, irregular-shaped $\text{Al}_7\text{Cu}_2\text{Fe}$ constituent particles exist in all product states, which indicates that intermediate heat treatments have little influence on this iron-caused, detrimental phase. The formation and evolution of microstructures for different product states of alloy 2195 were discussed in view point of the commercial production condition.

Key words: Al-Li alloy; commercial production; microstructure evolution; rolling; heat treatment

1 Introduction

Aluminum-lithium alloys, due to their low densities, have been regarded as competitive structural materials for aerospace applications[1–2]. The high-strength, weldable Al-Li alloy 2195 (Al-4.0Cu-1.0Li-0.4Mg-0.4Ag-0.12Zr, mass fraction, %) was developed to take the place of AA2219 which was conventionally used to build the huge external tank of USA space shuttles[3–4], and first achieved commercial application in NASA’s mission STS-91. In that launch, the super light weight tank built of 2195 plates provides a mass reduction of 3 175 kg and 50% increase of the payload capability for the shuttle. Because of the huge success, alloy 2195 has attracted worldwide attention.

So far, most researches on alloy 2195 have been focused on fundamental aspects[5–6], such as strengthening mechanism and microstructural design. As for studies at commercial level, HALES and HAFLEY[7], KALU and ZHANG[8] have investigated the texture evolution and anisotropic nature of several 2195 wrought products with commercial sizes, including near-net-shape extrusions, hot-rolled plates and ring roll

forgings. Their results show that alloy 2195 has complex evolutions of grain morphology, texture, through-thickness anisotropy when it undergoes multi-stage deformation. However, these investigations are associated with hot-deformed products only, and few are extended to further product states in which the cold working will be involved.

With a view to obtain some in-depth understandings about the microstructure evolution of alloy 2195 during the whole commercial production procedures, the present work has conducted an overall observation on microstructures of commercially fabricated 2195 plates and sheets, with product states covering hot rolling, cold rolling and artificial aging.

2 Experimental

2.1 Materials

Commercial fabrication of 2195 rolled products consists of a series of processing procedures, such as homogenization, hot rolling, intermediate annealing, cold rolling, solution treatment and quenching, cold-working and artificial aging, as schematically shown in Fig.1.

The slab of 3 000 kg, with thickness around 300

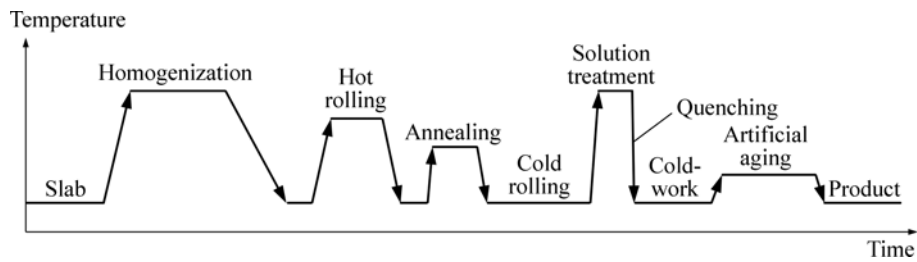


Fig.1 Schematic diagram of commercial production procedures of 2195 rolled product

mm was homogenized at temperature up to 495 °C, and then hot-rolled to plate of 10 mm in thickness at a 2 800 mm four-high, reversible hot-rolling mill. The plate was annealed and then cold-rolled to sheets with thickness ranging 2–5 mm at a 1 650 mm four-high, reversible cold-rolling mill. Sheets of 2 mm were solution treated in salt bath at 500 °C and quenched into water of room temperature, then cold-worked by 3% and artificially aged (T851 processing) at 160 °C for 2, 16 and 100 h, respectively, to achieve so-called under-aged, near peak-aged and over-aged products.

Three kinds of typical product states, i.e., hot-rolled plate of 10 mm, cold-rolled sheet of 5 mm and aged sheets (including three aging stages) of 2 mm, were selected to represent the primary processing procedures of commercial production. All specimens were taken from above-mentioned plates or sheets.

2.2 Experimental methods

As-rolled (hot-rolled and cold-rolled) products were optically observed on cross-sections along rolling, transverse and normal directions, respectively. Substructures from hot working or intermediate annealing were displayed using transmission electron microscopy(TEM). The precipitation behavior of aged products was studied by means of TEM and tensile test. Constituent particles inside products were analyzed by means of scanning electron microscopy(SEM).

Metallographic observation was performed under an Olympus-BHM optical microscope; TEM observation was performed on a Philips CM20 transmission electron microscope operated at 200 kV; SEM analyses were carried out with a JEOL-840A scanning electron microscope equipped with energy dispersive X-ray spectrometer (EDS) operated at 20 kV; and tensile test was carried out on an AG-IS 100 kN electronic tensile tester at room temperature with specimen orientation along the transverse direction of products.

3 Results and discussion

3.1 Microstructures of as-rolled products

Three-dimensional micrographs of as-rolled products are given in Fig.2. It can be seen from Fig.2(a)

that fibrous structure is the microstructural characteristic of hot-rolled product, similar to the result of HALES and HAFLEY[7]. The morphology on longitudinal section shows a uniform distribution of fibrous metal throughout the thickness of plate, and no obvious grain boundaries exhibit. This means that as-cast grains of the slab have been fully broken by the hot rolling of commercial scale which has a working amount more than 95%. Also because of the high strain rate of commercial rolling, few dynamically recrystallized grains are seen, which is in a good accordance with the previous work of the author[9].

Fig.2(b) shows a “pan-caked” grain structure in the cold-rolled product. Because the total working amount of cold rolling is much less than that of hot rolling, some recrystallized grains arising from intermediate annealing are partially remained after cold working. DU et al[10] have investigated the recrystallization behavior of 2195 plate during intermediate annealing. They found that the recrystallization nucleation in 2195 plate occurred heterogeneously in some planar zones parallel to rolling direction and recrystallized grain boundaries would

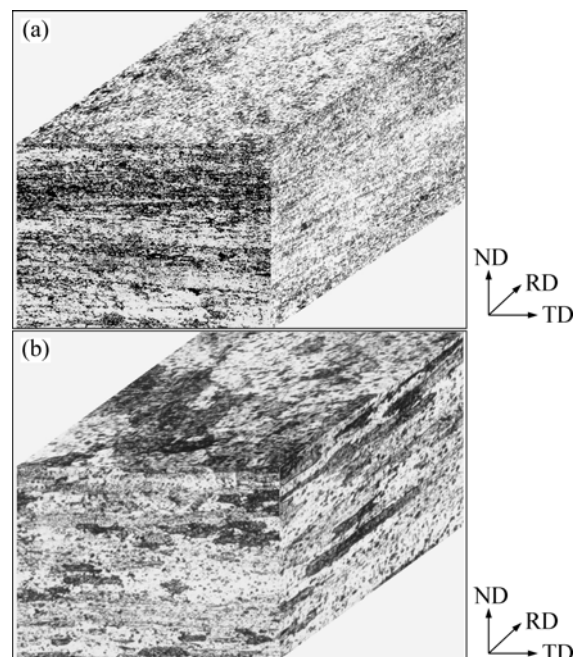


Fig.2 Three-dimensional micrographs of as-rolled products (RD—Rolling direction; TD—Transverse direction; ND—Normal direction): (a) Hot-rolled plate; (b) Cold-rolled sheet

interact with undissolved particles remaining in planar zones, which resulted in the formation of elongated grains. Therefore, the observed “pan-caked” grain structure of cold-rolled sheet should be, in some sense, the structural heredity of those elongated recrystallized grains of plate after intermediate annealing.

Fig.3 gives the TEM images of as-rolled products. The morphology of hot-rolled plate shown in Fig.3(a) exhibits fine, polygonized substructures. This gives the evidence that dynamic recovery is the main softening mechanism of alloy 2195 during commercial hot rolling. Fig.3(b) shows that the cold-rolled product contains high density dislocation cells, which should be attributed to the strong deformation at room temperature.

3.2 Precipitation behavior of aged product

Fig.4 shows morphologies of precipitates inside the aged products of alloy 2195 at different aging temps. It can be found that for 2 h aging at 160 °C, some fine $T_1(\text{Al}_2\text{CuLi})$ plates have precipitated on $\{111\}_\alpha$ planes of the aluminum matrix, and no $\theta'(\text{Al}_2\text{Cu})$ plates are observed, as shown in Fig.4(a). For near peak-aging of 16 h at 160 °C, a uniform dispersion of T_1 -plates exhibits, as shown in Fig.4(b). Besides T_1 -plates, a small

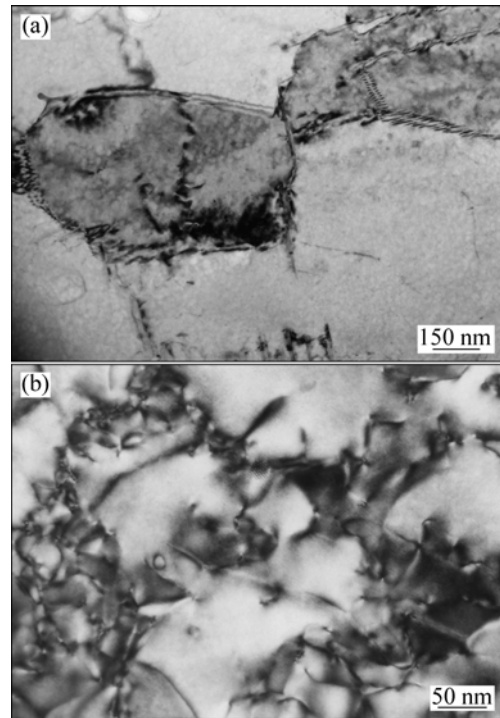


Fig.3 TEM morphologies of as-rolled products: (a) Hot-rolled plate; (b) Cold-rolled sheet

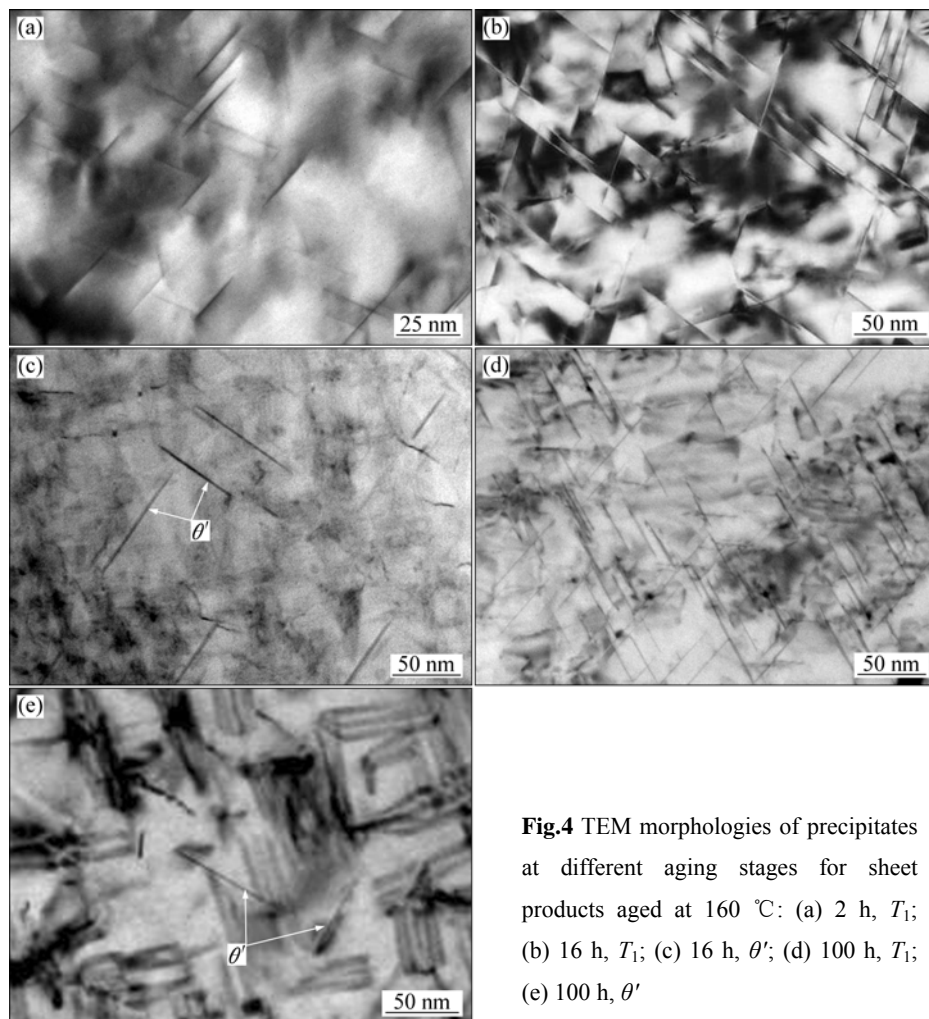


Fig.4 TEM morphologies of precipitates at different aging stages for sheet products aged at 160 °C: (a) 2 h, T_1 ; (b) 16 h, T_1 ; (c) 16 h, θ' ; (d) 100 h, T_1 ; (e) 100 h, θ'

fraction of θ' -plates are also observed on $\{100\}_\alpha$ planes, as given in Fig.4(c). For over-aging of 100 h at 160 °C, it can be seen that T_1 -plates have obviously coarsened (Fig.4(d)) and θ' -plates are much fewer (Fig.4(e)).

Fig.4 shows that the age-hardening response of alloy 2195 at 160 °C is dominated by the T_1 precipitation. θ' phase just plays the minor role in the precipitation strengthening of this alloy. This should be due to the relatively high aging temperature, 160 °C, at which the metastable θ' phase is supposed to need a longer incubation period for nucleating than the equilibrium T_1 phase. So, only T_1 phase precipitates under 2 h aging, but both T_1 and θ' can be seen on 16 h aging. With further aging, T_1 phase seems to grow or coarsen by consuming θ' phase, which can be confirmed by images of Figs.4(d) and (e). According to above results, the precipitation sequence of alloy 2195 at 160 °C aging can be taken as follows:

Supersaturated solid solution \rightarrow fine $T_1 \rightarrow$ dispersive $T_1 +$ a few $\theta' \rightarrow$ coarsened $T_1 +$ fewer θ'

A common feature with high strength aluminum alloys is the presence of plate-shaped, shear resistant precipitates formed on the $\{111\}_\alpha$ or $\{100\}_\alpha$ planes of the aluminum matrix. NIE and MUDDLE[11] have indicated that the strengthening effect produced by $\{111\}_\alpha$ plates (like T_1) is larger than that produced by $\{100\}_\alpha$ plates (like θ') and the best strengthening effect is associated with a continuous, three-dimensional network of dispersive, plate-shaped precipitates, similar to those shown in Fig.4(b). So, alloy 2195, containing both $\{111\}_\alpha$ T_1 -plates and $\{100\}_\alpha$ θ' -plates, can achieve a strength level much higher than its target alloy AA2219 which is only strengthened by θ' phase. Results of the tensile test show the near peak-aged 2195-T851 sheet possesses a mechanical property combination with the ultimate tensile strength of 565 MPa, the yield strength of 540 MPa and the elongation of 10.2%, which is well corresponding to its microstructural morphology.

MUDDLE and NIE[12] have concluded that the nucleation of strengthening precipitates in aluminum-based solid solutions is usually heterogeneous, and the heterogeneous nucleation is mostly associated with pre-existing structural defects such as dislocations, stacking faults and grain boundaries so as to reduce the obvious increase of interfacial or strain energies arising from the formation of nuclei. And it has been widely proved in Al-Cu-Li-X alloys that the cold-working prior to aging will introduce dislocations which act as favorable heterogeneous nucleation sites for precipitates like T_1 and θ' ; and hence, accelerate the age-hardening response of alloys[13–14]. Results of Fig.4 are well underpinning the above points of view.

3.3 Constituent particles inside products

By back-scattering technique of SEM, it is found

that there exist a large amount of secondary phase particles in all three product states, as shown in Fig.5. According to their shapes and sizes, it can be recognized that they belong to constituents which should have formed during solidification stage. Corresponding EDS analyses for those typical particles marked by white arrows in Fig.5 are given in Fig.6.

By comparing Fig.5(a) with Fig.5(b), it seems that the cold-rolled product has the more uniform distribution of particles than the hot-rolled one. This is because the cold-rolled product has been deformed more thoroughly. It is apparent in Fig.5(c) that the aged product has fewer

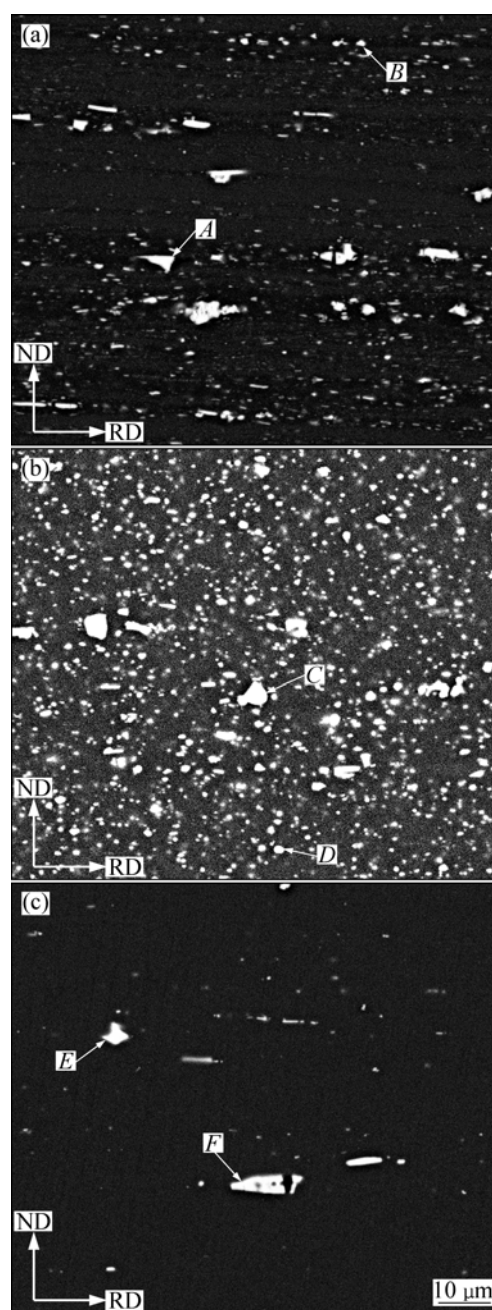


Fig.5 Back-scattering electron images displaying constituent particles existing inside all products: (a) Hot-rolled; (b) Cold-rolled; (c) Aged

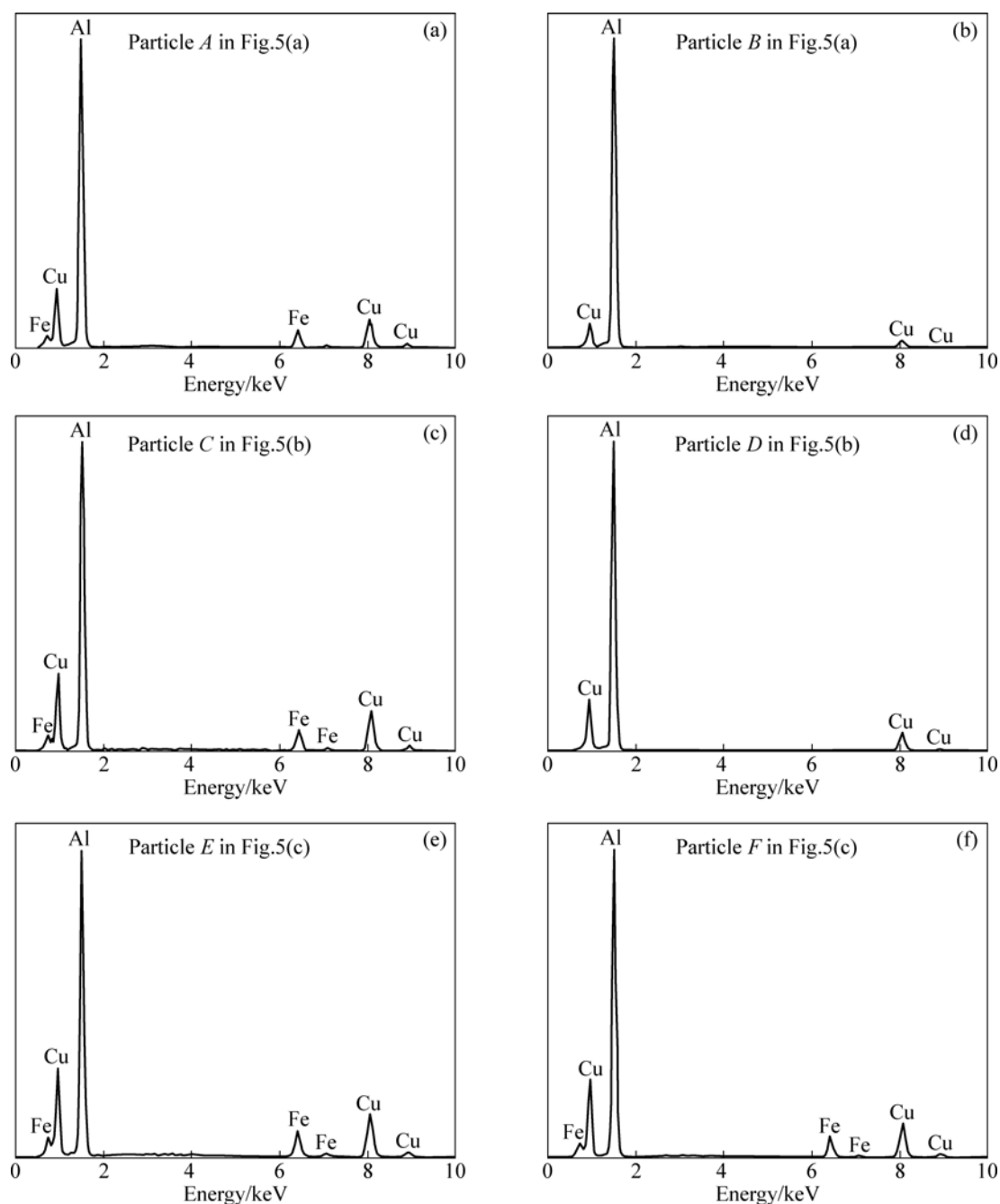


Fig.6 EDS analysis results for marked particles in Fig.5

particles than as-rolled product, which implies that the solution treatment has resulted in dissolving of quite a few particles. The EDS results show that the irregular-shaped, large-sized particles (particles *A*, *C*, *E*, and *F* in Fig.5) belong to the known $\text{Al}_7\text{Cu}_2\text{Fe}$ phase and the smaller-sized, round-shaped particles (particles *B*, *D* in Fig.5) belong to Cu-containing constituents. Of course, the constitution of these Cu-containing particles cannot be clarified because they may contain Li which cannot be detected by EDS.

It can be seen from Figs.5(a), 5(b) and their corresponding EDS results in Fig.6, the as-rolled products contain both $\text{Al}_7\text{Cu}_2\text{Fe}$ phase and Cu-containing

particles. From Fig.5(c) and its corresponding EDS results in Fig.6, only $\text{Al}_7\text{Cu}_2\text{Fe}$ particles are seen to remain in the aged product, and these Cu-containing particles should have dissolved into the $\alpha(\text{Al})$ matrix during solution treatment. The evidence of $\text{Al}_7\text{Cu}_2\text{Fe}$ phase existing in all product states means those intermediate heat treatments during commercial production, e.g. homogenization, intermediate annealing or solution treatment, have little influence on this iron-caused constituent which should have been brought in during solidification stage.

It has been known that $\text{Al}_7\text{Cu}_2\text{Fe}$ phase is a very deleterious constituent that will result in fatigue crack

initiation and localized corrosion of high-strength aluminum alloys which are mostly used as key structural materials in aircraft industries[15–16]. Also, the forming of $\text{Al}_7\text{Cu}_2\text{Fe}$ phase in large volume will undoubtedly consume some Cu atoms from the $\alpha(\text{Al})$ matrix and hence decrease the strengthening effect arising from any Cu-related precipitation, such as $T_1(\text{Al}_2\text{CuLi})$ or $\theta'(\text{Al}_2\text{Cu})$.

The fact of bulky $\text{Al}_7\text{Cu}_2\text{Fe}$ particles existing in commercial products of alloy 2195 suggests that the current technological capability of impurity control during its commercial production is still unsatisfactory. In further development of this alloy, more effective measures need to be taken, under the commercial scale, to reduce as much as possible any impurity-related, detrimental effect on the product quality.

4 Conclusions

1) The hot-rolled plate has a fibrous structure containing fine, polygonized substructures; and the cold-rolled sheet has a “pan-caked” grain structure containing high density dislocation cells.

2) 2195-T851 aged product is strengthened predominantly by a uniform dispersion of $\{111\}_\alpha$ $T_1(\text{Al}_2\text{CuLi})$ plates, and additionally by a small fraction of $\{100\}_\alpha$ $\theta'(\text{Al}_2\text{Cu})$ plates. The precipitation of T_1 or θ' is associated with dislocations introduced by the cold-working prior to aging.

3) There are many bulky, irregular-shaped $\text{Al}_7\text{Cu}_2\text{Fe}$ particles existing in all product states, i.e., these particles keep undissolvable during the whole commercial production procedures. Intermediate heat treatments have little change to the existence of this detrimental constituent.

Acknowledgements

This work was mostly performed in ARC Centre of Excellence for Design in Light Metals, Monash University, Australia. Special appreciations should be given to Prof. Barry C. MUDDLE, research director of the Centre, for his helpful advices on this work. One of the authors, JIANG Na, would like to thank the Monash Centre for Electron Microscopy (MCEM), for providing conveniences in carrying out microstructure analyses.

References

- [1] RIOJA R J. Fabrication methods to manufacture isotropic Al-Li alloys and products for space and aerospace applications [J]. *Materials Science and Engineering A*, 1998, 257(1): 100–107.
- [2] WARNER T. Recently-developed aluminium solutions for aerospace applications [J]. *Materials Science Forum*, 2006, 519/521: 1271–1278.
- [3] SANDERS J H. Investigation of grain boundary chemistry in Al-Li 2195 welds using Auger electron spectroscopy [J]. *Thin Solid Films*, 1996, 277(1/2): 121–127.
- [4] CHATURVEDI M C, CHEN D L. Effect of specimen orientation and welding on the fracture and fatigue properties of 2195 Al-Li alloy [J]. *Materials Science and Engineering A*, 2004, 387/389: 465–469.
- [5] HUANG B P, ZHENG Z Q. Independent and combined roles of trace Mg and Ag additions in properties precipitation process and precipitation kinetics of Al-Cu-Li-(Mg)-(Ag)-Zr-Ti alloys [J]. *Acta Materialia*, 1998, 46(12): 4381–4393.
- [6] XU Yue, GENG Ji-ping, LIU Yu-feng. Effect of rare earth elements on anisotropy and microstructure of Al-Li alloy 2195 sheets [J]. *Journal of Rare Earths*, 2006, 24(6): 793–796.
- [7] HALES S J, HAFLEY R A. Texture and anisotropy in Al-Li alloy 2195 plate and near-net-shape extrusions [J]. *Materials Science and Engineering A*, 1998, 257(1): 153–164.
- [8] KALU P N, ZHANG L. Texture evolution in Al-Li 2195 alloy during net shape roll forging [J]. *Scripta Materialia*, 1998, 39(2): 175–180.
- [9] JIANG Na, LI Jin-feng, ZHENG Zi-qiao, REN Wen-da, HAN Dong-feng. Simulation on flow stress of multi-pass hot deformation of 2195 Al-Li alloy [J]. *Rare Metal Materials and Engineering*, 2007, 36(6): 949–953. (in Chinese)
- [10] DU Yu-xuan, ZHANG Xin-ming, YE Ling-ying, LIU Sheng-dan. Evolution of grain structure in AA2195 Al-Li alloy plate during recrystallization [J]. *Transactions of Nonferrous Metals Society of China*, 2006, 16(2): 321–326.
- [11] NIE J F, MUDDLE B C. Microstructural design of high-strength aluminum alloys [J]. *Journal of Phase Equilibria*, 1998, 19(6): 543–551.
- [12] MUDDLE B C, NIE J F. Nucleation-mediated structural refinement and aluminium alloy design [J]. *Materials Science Forum*, 2006, 519/521: 191–196.
- [13] LEE E W, FRAZIER W E. The effect of stretch on the microstructure and mechanical properties of 2090 Al-Li [J]. *Scripta Metallurgica*, 1988, 22(1): 53–57.
- [14] JIANG Na, LI Jin-feng, ZHENG Zi-qiao, WEI Xiu-yu, LI Yan-fen. Effect of aging on mechanical properties and localized corrosion behaviors of Al-Cu-Li alloy [J]. *Transactions of Nonferrous Metals Society of China*, 2005, 15(1): 23–29.
- [15] PAYNE J, WELSH G, Jr CHRIST R J, NARDIELLO J, PAPA ZIAN J M. Observations of fatigue crack initiation in 7075-T651 [J]. *International Journal of Fatigue*, 2010, 32(2): 247–255.
- [16] BIRBILIS N, CAVANAUGH M K, BUCHHEIT R G. Electrochemical behavior and localized corrosion associated with $\text{Al}_7\text{Cu}_2\text{Fe}$ particles in aluminum alloy 7075-T651 [J]. *Corrosion Science*, 2006, 48(12): 4202–4215.

(Edited by YANG Bing)